Isotropy of drift mobilities in hydrogenated amorphous silicon

Homer Antoniadis* and E. A. Schiff
Department of Physics, Syracuse University, Syracuse, New York 13244-1130
(Received 11 March 1991)

We report transient photocurrent and time-of-flight measurements in undoped hydrogenated amorphous silicon (*a*-Si:H) for photocarrier motion both parallel and perpendicular to the thin-film growth axis. These measurements were analyzed to obtain the electron drift mobility and deep-trapping mobility-lifetime product at room temperature. We found good agreement of the electron-drift-mobility measurements for both field directions in two specimens prepared in several light-soaking states. Fifteen pairs of mobility-lifetime product estimates for the two field directions were also measured in a larger number of specimens. The data exclude an electron-transport anisotropy in *a*-Si:H greater than a factor of 2 in our specimens. We also studied the effects of absorption depth upon estimates of deep-trapping mobility-lifetime products for the standard sandwich electrode structure; results using 520-nm illumination yield estimates that are typically half the value estimated with uniformly absorbed illumination. We also present data on the correlation of the electron and hole deep-trapping mobility-lifetime products for these specimens.

I. INTRODUCTION

The transport of electrons in hydrogenated amorphous silicon (*a*-Si:H) is usually assumed to be isotropic—independent of the direction of the field.[1,2] However, *a*-Si:H thin films have a growth axis that might in principle give rise to anisotropic transport. Parker and Schiff reported a substantial anisotropy in the deep-trapping mobility-lifetime product for electron transport;[3] the drift mobility of the electrons prior to deep trapping was reported to be isotropic. Subsequently Kočka *et al.*[4,5] found a much smaller difference in mobility-lifetime products for the two transport directions, and concluded that electron transport was strictly isotropic through deep trapping. Bullot *et al.*[6] reported essentially isotropic steady-state photoconductivity in undoped *a*-Si:H, which essentially demonstrates that the mobility-lifetime product through recombination was isotropic.

The weight of the evidence thus favors isotropic electron transport in undoped Si:H, but several issues remain. Each of these three reports was based on study of single specimens, and thus the experimental case for isotropy is certainly not conclusive. Second, Kočka *et al.*[4] speculated that the claim of anisotropy by Parker and Schiff may have been due to their unconventional technique for measuring electron drift. In the present paper we address these issues. We have used the techniques of Parker and Schiff to study transport isotropy for a wider range of specimens and light-soaking states. All of these measurements supported isotropic transport of electrons.

The organization of this paper is the following. In Sec. II we briefly review the three principal interpretations of transient photocurrent measurements: (i) average drift mobilities obtained from photocarrier transit times, (ii) transient drift mobilities obtained from the transients prior to transit, and (iii) deep-trapping mobility-lifetime products determined by integration of transient photocurrents to obtain a photocharge. Our experimental procedures and specimens are described in Sec. III. In Sec. IV we present transport measurements for two electrode structures with transport parallel or perpendicular to the growth axis. Typical photocurrent transients and photocharge versus voltage data are presented showing electron time of flight for both field directions. We then analyze these data to obtain drift mobilities and mobility-lifetime products for both directions, and present a summary of these parameters for a wide variety of specimens and light-soaking states. In Sec. V we discuss the results and their implications for the isotropy of electron transport in *a*-Si:H. In the Appendix we further discuss the technique used for these drift-mobility measurements, which is based upon the use of uniform photogeneration of carriers. Conventional time of flight employs near-surface-absorbed illumination. We show that the estimates using uniform and surface-absorbed illumination are comparable, and we present auxiliary measurements on hole transport in our specimens which account for the success of measurements with uniform illumination.

II. TRANSIENT METHODS FOR EXPLORING ISOTROPY

A. Average drift mobilities and time of flight

The best known technique for measuring drift mobilities in amorphous semiconductors involves detection of photocarrier "time of flight."[7] A sheet of charges is generated near the top of a specimen using a laser impulse. The transit time t_T required for the sheet to traverse the interelectrode gap is determined by monitoring the photocurrent induced in an external bias circuit, and an average drift mobility μ_d is computed from t_T through the relation

$$\mu_d = \frac{d}{t_T E} , \tag{1}$$

where d is the electrode separation (in this case the thickness of the specimen) and E the applied electric field inducing the drift.

B. Difficulties in application of time of flight to isotropy

This time-of-flight procedure is not readily applicable to transport parallel to the surface of a thin-film material such as *a*-Si:H. Coplanar electrodes can be applied to the surface of the specimen, but it is difficult to generate a well-defined "pencil" of illumination near one of the electrodes. In addition, μ_d depends upon the gap d and the field E in materials with dispersive transport.[8] It is thus very cumbersome to compare values of μ_d obtained using differing fields or electrode gaps when dispersion obtains.

Kočka *et al.*[4] solved the first problem (photogeneration near one electron) by preparing a very small, parallelepiped specimen from the *a*-Si:H film and then using the conventional time-of-flight procedure with the sample aligned for two different transport directions. Parker and Schiff[3] used uniform illumination between the electrodes for both transport directions. The modifications of the procedure for analyzing transient photocurrents to obtain drift mobilities with uniform illumination were discussed both in their papers[3,9] and by Seynhaeve, Barclay, and Andriaenssens.[10] In our work we used the techniques of Parker and Schiff; in the Appendix we briefly review the necessary analysis, and we demonstrate that both surface and uniformly absorbed light give comparable transport results for transport in *a*-Si:H parallel to the growth axis.

C. Average and transient drift mobilities

The second problem—the superficial dependence of μ_d upon electrode separation and field when transport is dispersive—is fairly minor for electrons in *a*-Si:H, which are nondispersive at room temperature and above.[11–13] However, the problem can be obviated altogether by representing transient photocurrent data in terms of *transient* drift mobilities and mobility-lifetime products. These parameters are independent of electrode spacing and field (at least for regimes where transport depends linearly upon field[14]). In the remainder of this section we briefly describe these procedures and their relationship to the *average* drift mobility μ_d obtained from transit times.

Following a laser impulse at time $t=0$, a transient photocurrent $i(t)$ flows in the external voltage bias circuit due to the motion of the total photocarrier charge Q_0; we assume that only one type of photocarrier contributes to $i(t)$. The magnitude of $i(t)$ is calculable by equating the dissipation of the total photocarrier charge Q_0 drifting in the specimen by an external field E and the power supplied by the external bias voltage V:

$$i(t)V=Q_0 v(t)E \ , \tag{2}$$

where $v(t)$ will be the average drift velocity of the photocarriers. This equation is independent of the spatial distribution of photocarriers. If the time t is sufficiently short that few carriers have reached the counterelectrode, the drift velocity $v(t)$ is presumably proportional to the applied electric field E. We term the proportionality constant the *transient drift mobility:*

$$v(t)=\mu(t)E \ . \tag{3}$$

$\mu(t)$ is an intrinsic property of the material, independent of the electrode separation and field. The explicit dependence upon time of $\mu(t)$ is termed dispersion.[8] This time dependence in *a*-Si:H is often attributed to "multiple trapping" of the photocarriers by bandtails.[11–13,15,16]

Equations (2) and (3) can be combined to obtain an equation of the transient drift mobility $\mu(t)$ and a *normalized transient photocurrent* $i(t)d^2/Q_0V$:

$$\mu(t)=i(t)\frac{d^2}{Q_0 V} \ ; \tag{4}$$

d is the electrode separation and V the applied voltage bias. We eliminated E from Eq. (2) using $V=Ed$. The equation is valid in the limit that a negligible fraction of the total photocarrier charge Q_0 has arrived at the collecting electrode. An important aspect of Eq. (4) for the present work is that it is valid for arbitrary absorption profiles—including conventional near-surface illumination and uniform illumination.

The relation of $\mu(t)$ and μ_d has been discussed by Tiedje[11] and by Parker and Schiff;[3] the latter showed a good experimental correlation between direct transit-time t_T measurements of μ_d and estimates of μ_d from the average of $\mu(t)$ over the integral t_T:

$$\mu_d=\frac{1}{t_T}\int_0^{t_T}\mu(t)dt \ . \tag{5}$$

D. Estimating Q_0 from charge-collection measurements

In order to use Eq. (4) to estimate $\mu(t)$ the total photocarrier charge Q_0 must be determined. This is usually done using the photocharge $Q(t)=\int_0^t i(t')dt'$ which has flowed through the external bias circuit since $t=0$. The photocharge $Q(t)$ measures the mean drift $x(t)$ of the photocarrier distribution,[17,18] as is clear from integration of Eq. (2):

$$Q(t)V=Q_0[x(t)-x(0)]E \ . \tag{6}$$

For sufficiently large voltages the displacement $x(t)$ saturates at the value of the electrode spacing $x(t)=d$, since d is the maximum possible value of x. Q_0 can then be obtained from the saturation value.

E. Mobility-lifetime products

Charge-collection data are also often used to estimate mobility-lifetime products $\mu\tau(t)$ as well as Q_0.[18–25] We briefly describe the relationship of these mobility-lifetime products to $\mu(t)$; the issue is discussed in more detail elsewhere.[26,23] These mobility-lifetime products are determined using charge-collection measurements at lower voltages, where a linear relationship between $Q(t)$ and V exists:[18,19,21]

$$Q(t)=Q_0\mu\tau(t)\frac{V}{d^2}\ . \tag{7}$$

We have generalized the definition of a mobility-lifetime product to incorporate the possibility that the charge-collection curves depend upon the collection time.[26,18,25,28,29] Comparison of Eqs. (6) and (7) shows that they are consistent if $x(t)/E=\mu\tau(t)$: that is, the displacement $x(t)$ depends linearly upon electric field. In this low-field limit Eq. (3) [$v(t)=\mu(t)E$] also applies, from which we obtain that

$$\frac{x(t)}{E}=\int_0^t\frac{v(t')}{E}dt'=\int_0^t\mu(t')dt'\ . \tag{8}$$

We can therefore equate the mobility-lifetime product $\mu\tau(t)$ determined from charge-collection measurements with $\int_0^t\mu(t')dt'$.[26]

III. SPECIMENS AND INSTRUMENTATION

A. Specimens

a-Si:H specimens were deposited using a commercial (Plasma Technology, Inc. "Plasmalab") 13.56-MHz rf plasma reactor operating with 200 mT of pure silane gas at 5 W of rf power. Specimens were deposited onto Corning 7059 glass substrates; substrate temperatures were varied from 160 to 350 °C. The densities of paramagnetic D centers were measured using electron-spin-resonance spectroscopy.[24] In Table I we list some details for the specimens used in these experiments.

B. Electrode structures

We explored transient photocurrents for electric fields in the directions illustrated at the top of Fig. 1. "Axial" fields are parallel to the growth axis of the thin film; "planar" fields are perpendicular to this axis.

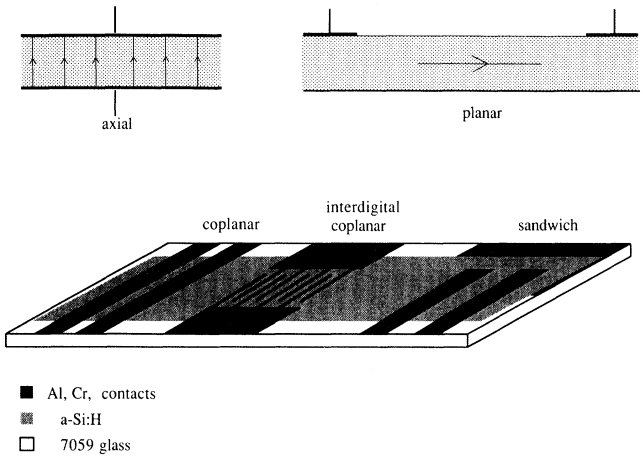

FIG. 1. Schematic illustration of the three types of electrode structures used for this research; drawings are not to scale. The upper portion of the figure illustrates the direction of axial and planar electric fields relative to the growth axis of the thin film.

In Fig. 1 we have illustrated the three electrode configurations used for these experiments. The bottom electrode of the sandwich configuration was evaporated chromium. Following deposition of the *a*-Si:H layer, a semitransparent aluminum top electrode was evaporated. The top electrode had an optical density of about 1.5 and overlapped the bottom electrode over about 2 mm^2. We had no serious difficulties with electrical shorting of these structures by pinholes.

TABLE I. Summary of some properties of the specimens used: T_s, substrate deposition temperature; d, thickness of the specimens; N_S, density of paramagnetic defect centers D^0 measured with electron spin resonance; $\mu\tau_{e,t}$, electron deep-trapping mobility-lifetime product; and $\mu\tau_{h,t}$, hole deep-trapping mobility-lifetime product. Both $\mu\tau$ products are measured in the sandwich electrode geometry and correspond to 10 μs collection time (unless otherwise indicated). Electron measurements were done using about 680-nm illumination (uniformly absorbed). Hole measurements were done using 520 nm (surface absorbed). In the sample numbers AN stands for annealed, LS for light soaked, and B for baked.

Sample number	T_s (°C)	d (μm)	N_S (cm^{-3})	$\mu\tau_{e,t}$ (cm^2/V)	$\mu\tau_{h,t}$ (cm^2/V)
(1223AN)	250	10.3	3.5×10^{15}	3.5×10^{-7}	1.2×10^{-8} (1 ms)
(1223LS1)	250	10.3	8.1×10^{15}	2.1×10^{-7}	
(1223LS2)	250	10.3	1.2×10^{16}	1.3×10^{-7}	
(1223LS3)	250	10.3	2.0×10^{16}	6.1×10^{-8}	
(JUNAN)	250	3.8	$\sim3\times10^{15}$	1.8×10^{-7}	$\geq8.0\times10^{-9}$ (300 μs)
(NOVAN)	250	3.3	$\sim3\times10^{15}$	$\geq1.5\times10^{-7}$	
(314AN)	350	2.0	7.9×10^{15}	1.8×10^{-7}	3.7×10^{-9}
(314LS)	350	2.0	1.4×10^{16}	3.1×10^{-8}	
(316AN)	350	0.8	2.0×10^{16}	9.4×10^{-9}	
(316LS)	350	0.8	2.3×10^{16}	7.5×10^{-9}	9.6×10^{-10}
(413AN)	195	1.5	1.2×10^{17}	6.8×10^{-9}	2.9×10^{-10}
(411AN)	175	1.0	1.8×10^{17}	5.4×10^{-9}	2.2×10^{-10}
(46AN)	160	0.9	3.9×10^{17}	5.4×10^{-10}	7.2×10^{-11}
(46ANB)	170	0.9		6.7×10^{-9}	

The planar contacts were evaporated onto the *a*-Si:H film following deposition. The interdigital electrodes were prepared using the photolithographic procedures previously described by Parker and Schiff.[3,30] We used chromium for these electrodes; we experience difficulty with liftoff procedures using aluminum top electrodes. The gap between the interdigital electrodes was 30 μm; there were 20 digits for each pad. We also used standard pairs of coplanar electrodes; the gap between the electrodes was 500 μm. Both aluminum and chromium were used for these pairs.

We verified for all cases that the transient response of these electrode structures was not limited by the electrode resistance. The thickness of the interdigital electrodes needed to be as thin as possible to simplify the photolithographic liftoff procedure. We measured the dark currents for these electrodes in response to bias-voltage steps similar to those used for the transient photocurrent measurements reported in the next section. Both voltage polarities were examined; the transient injection and dielectric relaxation currents were negligible in comparison to the transient photocurrents reported in the next section. We presume that the metal-semiconductor interfaces acted as Schottky diodes over our time regime; the structures were thus "back-to-back" diodes.

C. Light soaking

Some of our measurements were performed upon specimens that had been "light soaked" (exposed to extended illumination prior to the transient measurements). The illumination source was a type-ENH tungsten halogen bulb used at a distance of 30 cm from the specimen (incident illumination about 300 mW/cm^2).

It is important that the region of *a*-Si:H between the electrodes receive comparable illumination for all types of electrode structures. The sandwich electrode structures have a top electrode which attenuates the illumination received by this structure, whereas coplanar electrode structures receive illumination directly. In addition the sandwich electrode structure has a reflective back electrode not present for the coplanar specimens.

We compensated for the absence of a back electrode for the coplanar specimens by placing them on a reflective pedestal during light soaking. We followed two procedures to compensate for the presence of the top electrode in sandwich structures. The first procedure involved fabrication of a compensating filter. When the top electrode was deposited onto a sandwich structure, a second metal film was codeposited onto a glass slide. This slide was placed in front of the coplanar electrode structure during light soaking to compensate for the top electrode of the sandwich structure. The second procedure was to light soak the specimen prior to deposition of the top electrode.

D. Transient photocurrent measurements

Transient photocurrents measurements were performed using a commercial nitrogen laser pumped dye laser (Laser Science, Inc. model VSL-DCM-1, with integral rf shielding). The wavelength range accessible with this laser is 440–700 nm; the pulse duration was 3 ns. The laser intensity was measured using a beamsplitter and a standard Si *p-i-n* photodiode.

Photocurrents in the structure passed into a 100-MHz bandwidth amplifier (50 Ω impedance). The amplified wave form was recorded and averaged using a 125-MHz bandwidth digital oscilloscope (LeCroy, Inc. model 9400). This oscilloscope was interfaced to a personal computer for storage and analysis of the transient wave forms.

The bias voltage was applied to a structure at least 1 μs prior to the laser flash. The transient charging of the structure in response to the voltage and light pulses was measured by using a *RC* integrator. As noted earlier, the dielectric relaxation and electrode effects were negligible on our time scale. The photocharge was kept below 10% of the *CV* charge, and we concluded that the photocarriers did not appreciably screen the external field. For laser repetition rates greater than 1 Hz we found "build-up" of charge in the material in some cases; the measurements reported here were performed at rates smaller than this threshold.

E. Optical calibration procedures

In several cases we estimated the number of photons absorbed between the specimen's coplanar electrodes using a commercial Si *p-i-n* diode. We calculated the laser pulse intensity (photons per unit area) from the detector's specifications. The number of photons absorbed by the sample was obtained from this intensity estimate, the electrode geometry, and a correction for the specimen's reflectivity at normal incidence and its absorption length at the laser wavelength. To improve the accuracy of these estimates we used laser wavelengths which were nearly completely absorbed by the specimen when optical calibration was necessary.

IV. RESULTS

In this section we first present transient photocurrent measurements for sandwich and interdigital electrode structures. We selected a wavelength for these experiments such that the absorption of light was uniform or nearly so through the material. The use of uniform illumination is a departure from conventional time-of-flight techniques. It permits the results of interdigital and sandwich electrodes to be compared, but it opens up the possibility of a hole contribution to the transient photocurrents. We show in the Appendix that the transients for sandwich electrodes with uniform illumination give essentially the same results as with conventional electron time of flight, and that hole transport was small.

In Sec. IV A we present the transients measured with both electrode structures; electron time of flight was observed for both. In Sec. IV B we present photocharge collection measurements; these are consistent with time-of-flight data, and were used to obtain the total photocarrier charge Q_0 and also the deep-trapping mobility-lifetime product for electrons $\mu\tau_{e,t}$. In Sec. IV C we

present our estimates of the transient drift mobility $\mu_e(t)$ and deep-trapping mobility-lifetime products $\mu\tau_{e,t}$ for electrons based on the measurements for both electrode structures. We find that these estimates generally support isotropic transport for electrons in this material.

A. Axial and planar transient photocurrent measurements

In Fig. 2(a) we show the electron photocurrent transients measured using a sandwich electrode structure for several electric fields. The measurements were at room temperature; the specimen was in its annealed state. The electric fields inducing the drift of the photocarriers in this geometry are parallel to the growth axis of the specimen (cf. Fig. 1). The laser wavelength was 684 nm, which is absorbed nearly uniformly in this specimen (about 10 μm thickness). In Fig. 2(a) the photocurrent transients have been normalized by the bias voltage V and the specimen's thickness d. In addition we have normalized the transients using our estimates of the total photocarrier charge Q_0 generated by the laser flash; the measurements used to determine Q_0 are presented in the next section.

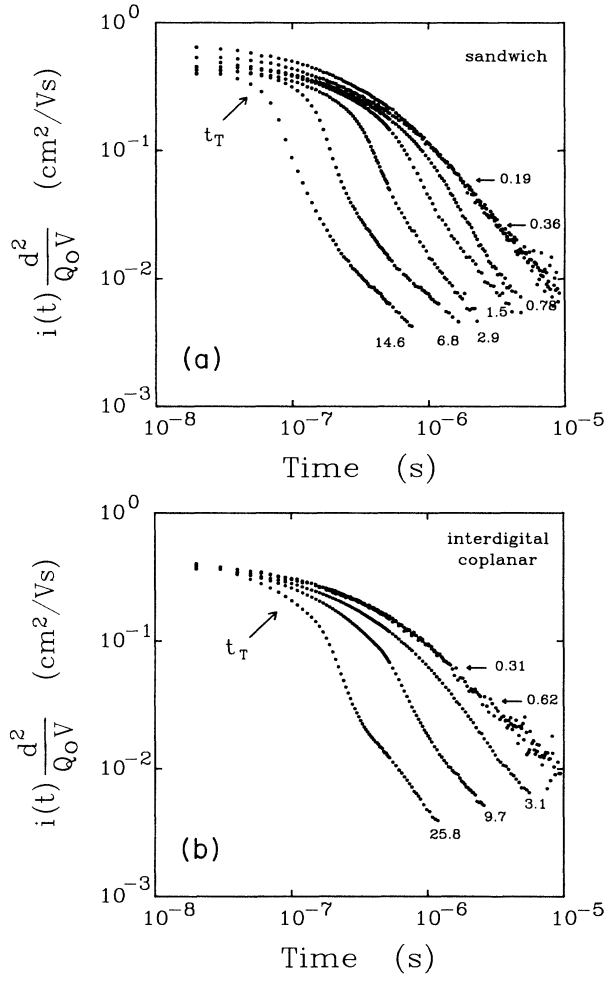

FIG. 2. Normalized photocurrent transients $i(t)d^2/Q_0V$ for an annealed a-Si:H specimen (cf. sample 1, Table I) at room temperature for a variety of electric fields (noted in units of kV/cm); illumination wavelength was 684 nm (uniformly absorbed). (a) Transients measured with sandwich electrodes. (b) Transients measured with interdigital coplanar electrodes. At high electric fields ($E>2$ kV/cm) the transients indicate sweepout of electrons; the transit time t_T is indicated by an arrow for the largest electric field. Note the near convergence of the transients for times less than the transit time.

In Fig. 2(b) the photocurrent transients are shown for interdigital coplanar electrodes on the same specimen using the same illumination wavelength; the electric field inducing the drift is essentially perpendicular to the growth axis (cf. Fig. 1).

The normalized photocurrent transients shown for the two electrode structures in Figs. 2(a) and 2(b) have the appearance expected for a time-of-flight experiment. At the earliest times all fields give approximately the same value of $i(t)d^2/Q_0V$. At these times no electrons have been lost to sweepout, and hence the photocurrents are expected to scale linearly with voltage. This Ohmic behavior is quite clear for the interdigital electrode structure. It is less apparent for the sandwich structure. For these structures substantial photocurrents are observable even at $V=0$ due to internal fields near the electrodes.[31] Such internal field transport always spoils the Ohmic scaling of the photocurrent for sufficiently small voltages. Internal field effects on photocharge measurements will be discussed in more detail subsequently.

At longer times the form of the transients reveals electron sweepout; as the electric field is increased successive curves depart from a common asymptote at earlier times due to the earlier onset of sweepout effects. We have indicated the transit time t_T for the highest voltage transient. A very similar approach was used by Marshall, Street, and Thompson[12] in their analysis of transient photocurrents to obtain transit times, with the exception that they used arbitrary scaling of the transients. In Sec. IV C we shall present our estimates of the electron drift mobility based on these transients.

B. Charge collection in axial and planar geometry

In Fig. 3 the electron photocharge Q collected at 10 μs is shown as a function of V/d^2 for the transients shown in Fig. 2. V is the applied voltage and d the interelectrode distance. These photocharge measurements essentially confirm the time-of-flight interpretation of the photocurrent transients described in the previous section. Two separate regions are obvious from the plot

(1) At high applied voltages the photocharge shows saturation. For these voltages all the electrons were swept out of the structure within 10 μs, and hence the charge is constant.

(2) At lower voltages the collected photocharge depends linearly on the voltage. Because electron sweepout is negligible in this limit, both the photocurrents and photocharges are expected to depend linearly upon the voltage bias.

Plots like the one shown in Fig. 3 are often used to esti-

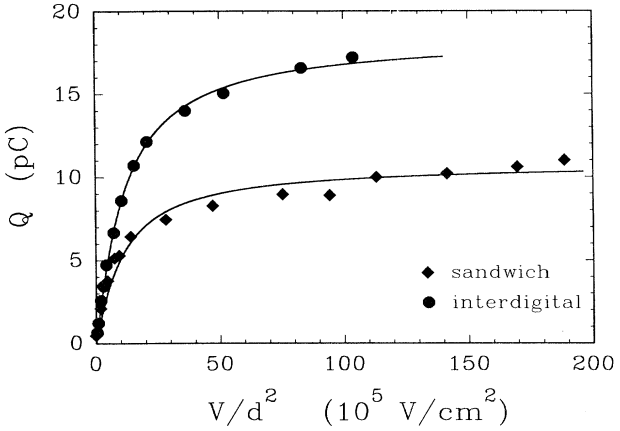

FIG. 3. Photocharge Q collected at 10 μs as a function of the externally applied voltage V (plotted as a function of V/d^2 where d is the interelectrode distance) for both electrode structures of sample 1 (cf. Table I). Electron motion dominates these measurements. The lines are fits using a Hecht analysis adjusted for unifrom generation of carriers (Ref. 30). The electron deep-trapping mobility-lifetime products obtained from the fits were $\mu\tau_{e,t}^{ax}=3.5\times10^{-7}$ cm^2/V and $\mu\tau_{e,t}^{pl}=3.3\times10^{-7}$ cm^2/V.

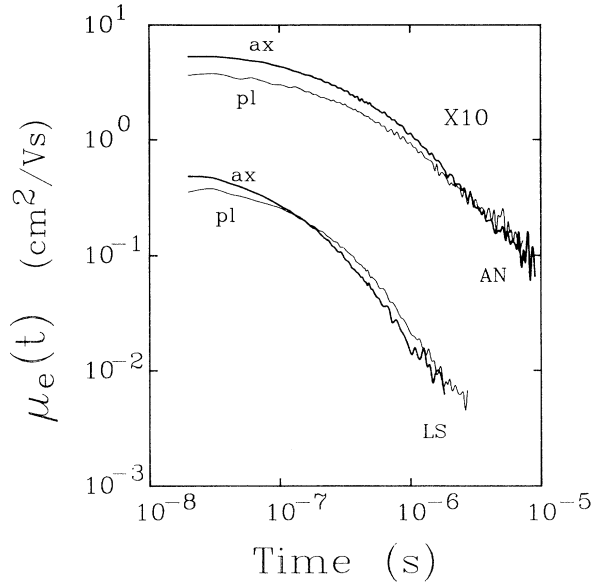

FIG. 4. Transient drift mobiities $\mu_e(t)$ measured using axial (ax) and planar (pl) electric fields. The curves denoted AN correspond to the annealed state of sample 1 also used for Figs. 2 and 3. The curves labeled LS refer to a light-soaked state of the same specimen (cf. sample 3 in Table I). The curves for the annealed state (AN) have been multiplied by ten for clarity.

mate the total photocarrier charge Q_0 and a deep-trapping mobility-lifetime product $\mu\tau_t$.[19,18] In conventional time-of-flight experiments the saturation photocharge is equal to the value of Q_0, the total charge generated by the laser flash. This procedure must be modified somewhat to correct for the use of uniformly absorbed illumination;[3,30] we show in the Appendix that Q_0 is twice the saturation value of the photocharge for these data.

At lower voltages (where $Q \ll Q_0$) the slope of the charge-collection curve can be used to estimate a mobility-lifetime product [compare Eq. (7)]:

$$Q=Q_0\mu\tau\frac{V}{d^2}\ . \tag{9}$$

For the case of nondispersive transport the form of this curve is also readily predicted. Hecht obtained the result for surface-absorbed illumination as well as for uniformly absorbed illumination.[32] For uniform illumination and one species of mobile carrier the collected photocharge will be given by the relation

$$Q=Q_0\mu\tau\frac{V}{d^2}\left\{1-\mu\tau\frac{V}{d^2}\left[1-\exp\left[-\frac{d^2}{\mu\tau V}\right]\right]\right\}\ . \tag{10}$$

This result was also obtained independently by Parker.[30] The relation above was used to fit the data of Fig. 3. We attribute the small systematic difference between the fit and the data to hole transport. We remind the reader that mobility-lifetime product estimates obtained using these procedures depend in principle upon the collection time;[26] related measurements have been reported in Refs. 25, 18, 29, and 28.

C. Isotropy

1. Drift-mobility estimates

Transient photocurrent data such as those presented in Fig. 2 are typically used to extract average drift mobilities μ_d using transit-time estimates. As noted in Sec. II, we preferred to express our results in terms of the transient drift mobility $\mu(t)$. $\mu(t)$ can be equated to the normalized photocurrent transient $i(t)d^2/Q_0V$ at times less than the transit time. In Fig. 4 we illustrate the electron transient drift mobilities $\mu_e(t)$ based on the transients of Fig. 2 (AN); we have also included estimates of $\mu_e(t)$ from additional data on the same specimen following light soaking (LS).

We first discuss how we obtain an estimate of planar $\mu_e(t)$ using the transients presented as Fig. 2(b); the results are presented as the upper curve with the label "pl" in Fig. 4. For the data of Fig. 2(b) a fairly good estimate of $\mu_e(t)$ is given directly by the normalized photocurrents for electric fields smaller than 0.8 kV/cm. In these lower fields the transient photocurrents were proportional to voltage for the entire range of times shown; the two normalized photocurrent transients shown in the figure are essentially indistinguishable. At higher fields $i(t)d^2/Q_0V$ agrees with the low-field estimate until the electrons are swept out.

The decay at long times $t>1$ μs in Fig. 4 is *not* an artifact of carrier sweepout; it is due to electron deep trapping[18–27] of the photocarriers before they traverse the specimen. At shorter times the time dependence of $\mu_e(t)$

is much weaker, consistent with the nondispersive transport of electrons in *a*-Si:H reported near room temperature in conventional time-of-flight drift-mobility measurements.[11–13]

The electric field in the thin film for coplanar electrodes is not strictly uniform. In Sec. II we assumed a uniform electric field to derive the relationship of $\mu(t)$ and $i(t)d^2/Q_0V$. Although a correction factor is calculable in principle, we have neglected this effect. We estimate that this leads to less than a 20% error in estimation of $\mu(t)$.

Estimated of $\mu_e(t)$ from the data for sandwich electrodes (upper curve labeled "ax" in Fig. 4) is more problematic. Long times present no difficulties: as for the interdigital electrode measurements in Fig. 2(b), the transients for $E < 0.4$ kV/cm superpose quite well. At short times there is no clear limiting curve such as is found in Fig. 2(b); we attribute the difficulty to internal field effects. We are unaware of any completely satisfactory procedure for correcting for the effects of internal fields.

We also measured photocurrent transients for both structures following light soaking (LS) (cf. sample 3 in Table I). We had no difficulties with internal fields following light soaking, and have directly presented our estimates of $\mu_e(t)$ in Fig. 4 without the supporting transient measurements.

For both states of this specimen the similarity of $\mu_e(t)$ for the two electrode structures appears consistent with isotropy of electron transport. The small disagreement of the transients between the two geometries is in our view consistent with the systematic errors of our techniques (nonuniform fields for interdigital electrodes, internal fields for sandwich electrodes).

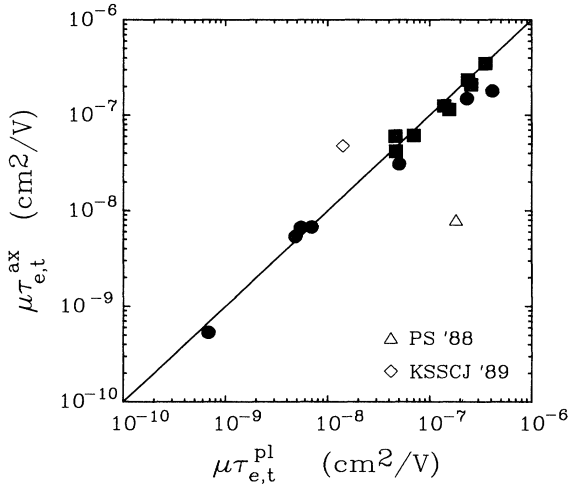

FIG. 5. Correlation of electron deep-trapping mobility-lifetime products $\mu\tau_{e,t}$ for a variety of undoped *a*-Si:H specimens measured with two electrode geometries. $\mu\tau_{e,t}^{ax}$ was measured using sandwich electrodes. $\mu\tau_{e,t}^{pl}$ was measured using two kinds of coplanar electrodes: interdigital (■) and conventional gap cell (●). The measurements of Parker and Schiff (PS) (Ref. 3), as well as of Kočka *et al.* (KSSCJ) (Ref. 4), are also included in the graph.

2. *Deep-trapping mobility-lifetime products*

We also examined the electron deep-trapping mobility-lifetime product estimated from charge-collection measurements on the two types of structures. Such measurements are much less time consuming than drift-mobility measurements, and thus appear to be well suited to a survey of many specimens for transport isotropy.

In Fig. 5 we have correlated the electron deep-trapping mobility-lifetime products $\mu\tau_{e,t}$ for the sandwich and coplanar electrode structures. We followed the procedure described in Sec. IV B for these estimates; however, for several specimens complete collection of charge within 10 μs was not possible due to our use of large gaps between coplanar electrodes (solid circles in Fig. 5). In these cases we estimated Q_0 from measurements of the incident laser intensity and the optical properties of the specimens; the optical calibration procedures were described previously. The specimens span a wide variety of paramagnetic defect densities (shown in Table I).

We have also included the related measurements of Parker and Schiff[3] and of Kočka *et al.*[4] in Fig. 5.

V. DISCUSSION

These data broadly confirm isotropy of electronic transport in *a*-Si:H. Figure 4 indicates that the transient drift mobilities $\mu(t)$ for two light-soaking states of one specimen were essentially the same for both directions of transport. In Fig. 5 most of the points indicate equivalence of the electron deep-trapping mobility-lifetime products $\mu\tau_{e,t}$ for the two types of structure and the two field directions; we remind the reader that the mobility-lifetime product is essentially the integral of $\mu(t)$ past the deep-trapping time. Several of the $\mu\tau_{e,t}$ points do indicate differences in estimates of $\mu\tau_{e,t}$ for the two types of structure. In this section we discuss some of the limitations of the experimental procedures used for these measurements and assess the data for which measurements in the two geometries were inequivalent.

The three sources for systematic error which we have assessed are (i) internal field effects near interfaces, (ii) use of optical calibration instead of complete photocarrier collection for determination of the photocharge Q_0, and (iii) light-soaking techniques.

We have found no satisfactory technique for extracting drift-mobility information in the presence of substantial internal field motion. We suggest that a practical criterion for the unimportance of internal fields is that the total average drift x_i due to internal fields between photogeneration and the measurement time should be much less than the drift due to external fields. This criterion largely explains the widespread use of rather thick specimens of *a*-Si:H for drift-mobility studies, since depletion layers in device-grade material can exceed 1 μm in depth.[31,33] It is also consistent with thickness dependence studies for coplanar electrode structures showing that bulk properties are observed in device-grade *a*-Si:H for thicknesses greater than 2 μm.[34]

For sandwich electrodes charge-collection data such as

those of Fig. 6(a) (see Appendix) can be used to estimate internal field drift; the intercept $Q(0)$ at $V=0$ indicates the distance through which electrons were translated by internal fields. For all the sandwich electrode data reported in Fig. 5 $Q(0)$ was small. We discuss these effects further in the Appendix.

For coplanar electrodes we believe the planar fields due to the electrodes are unimportant; the interelectrode gaps were very much larger than our estimates of Schottky barrier widths. However, vertical motion of the photocarriers in internal fields due to the top or bottom interfaces of the film might influence the data. We have no effective diagnostic procedure for these vertical motions. We would not expect the electron depletion layers usually reported near these interfaces[35,36] to substantially affect our measurements; electron accumulation layers might affect them[37] if their widths were comparable to the specimen's thickness.

As illustrated in Fig. 5, Kočka *et al.*[4] found a modest inequivalence for their two structures. In these experiments photogeneration of carriers occurred in regions near the electrodes; we therefore speculate that differing Schottky barriers in their two structures led to the observed discrepancy between $\mu\tau_{e,t}$ in their two structures.

The second possible source of systematic error which we considered is the use of optical calibration techniques (solid circular symbols in Fig. 5) to obtain the planar estimate $\mu\tau_{e,t}^{\rm pl}$. The optical calibration procedure is fairly elaborate, and we consider the optically calibrated points to be less reliable than those based on complete charge collection with interdigital electrodes (solid square symbols). The results in Fig. 5 nonetheless seem fairly consistent for the two procedures; we did not explicitly compare the two calibration procedures using interdigital electrodes.

Finally we note that several of the $\mu\tau_{e,t}$ pairs in Fig. 5 were obtained for light-soaked specimens, including the earlier estimate of Parker and Schiff. If we presume this earlier measurement is erroneous, we speculate that difficulty in obtaining comparable light soaking in the two structures is the most likely source of error.

We draw the following conclusion from the research presented here. Estimates of the electron deep-trapping mobility-lifetime product in *a*-Si:H for two types of electrode structure and several measurement techniques (differing in optical absorption length and calibration procedures) appear to be consistent within a factor of 2 or somewhat better. We believe that transport anisotropies larger than this can be excluded from the data. The work also shows that procedures for estimating $\mu\tau_{e,t}$ using coplanar electrode structures are as reliable as more conventional procedures using sandwich structures.

Research on the isotropy of $\mu\tau_{e,t}$ was started as one avenue for resolving the large ratio (of order 100) between conventional $\mu\tau_{e,t}$ measurements and estimates of the recombination mobility-lifetime product $\mu\tau_{e,r}$ based on steady-state photoconductivity measurements with coplanar electrodes.[25,26,38–40] Clearly anisotropy is insufficient to resolve this issue. Recently we have extended the research on coplanar electrode structures reported here to very long times ($t \gg 10$ μs). We find substantial further drift of electrons noticeable after 1 ms. Using these long-time transient techniques estimates we obtained estimates of $\mu\tau_{e,r}$ which were quite comparable to those obtained by steady-state measurements.[25] In our view these measurements show that the origin of the mobility-lifetime product discrepancy is simply due to the differing time scales of the measurements.

ACKNOWLEDGMENTS

The authors thank Steve Hotaling for depositing and characterizing most of the specimens, Mike Parker for instruction in the use of the equipment he built, and Kevin Conrad for many hours of help with and discussions of these experiments. The research was supported by the Solar Energy Institute through Subcontract No. XB-6-06005-2.

APPENDIX: DETERMINING $\mu\tau_{e,t}$ USING HOMOGENEOUS ILLUMINATION

In Sec. IV we presented results on the isotropy of $\mu\tau_{e,t}$ based on measurements with illumination which was absorbed uniformly between the electrodes. This procedure is unconventional; $\mu\tau_{e,t}$ is usually measured using surface-absorbed illumination and "sandwich" electrode geometry. In this appendix we show that the two procedures gave comparable results for sandwich electrodes, which is possible because holes are significantly less mobile than electrons in *a*-Si:H. Parker reached a similar conclusion in earlier, unpublished work.[30]

We first briefly describe the effects of using surface-absorbed or uniform illumination for materials with a single mobile carrier. A more comprehensive treatment of these effects is given in Refs. 30 and 41. Relation (6) is

$$Q(t)V = Q_0[x(t)-x(0)]E \ . \tag{A1}$$

This expression equates the energy supplied by the external bias supply with the work done by the electric field E in moving the total photocarrier charge Q_0 a distance $x(t)-x(0)$ inside the specimen.

The principal difficulty imposed by the use of illumination which is not surface absorbed is the determination of Q_0 from the experimental charge-collection data. The maximum collected charge $Q_{\rm max}$ measured after the carriers have been swept out of the specimen is

$$Q_{\rm max} = Q_0\left[1-\frac{x(0)}{d}\right] . \tag{A2}$$

Note that we have assumed that only one type of carrier contributes to $Q(t)$; to derive this relation we used (A1) and assumed a homogeneous electric field ($E=V/d$).

We shall need only the two special cases of surface and uniform absorption. For the first case the initial mean position of the photocarrier distribution will be $x(0) \ll d$, and the result $Q_{\rm max}=Q_0$ obtains. For uniform absorption the mean initial position is at the middle of the specimen: $x(0)=d/2$. Hence $Q_{\rm max}=Q_0/2$.

Using these arguments, we now discuss our measure-

ments of charge collection using surface- and bulk-absorbed illumination. In Fig. 6(a) we show the charge collected at 50 μs following photogeneration as a function of the applied voltage V. We used an a-Si:H specimen in a Schottky diode structure: Al/a-Si:H/Cr (cf. Sample 5 in Table I). 520 nm is absorbed near the surface; 684 nm is uniformly absorbed. The charge measurements were normalized to agree approximately with the discussion of charge collection just given. In Fig 6(b) we have enlarged the part of Fig. 6(a) close to the region of $V=0$ V in order to demonstrate better the charge collection at these low voltages.

The charge collection with surface-absorbed light is quite different for the two voltage polarities. For negative bias voltage electron motion dominates; for positive bias voltage hole motion dominates. As mentioned earlier in Sec. III the $\mu\tau$ products corresponding to 50 μs can be estimated for electrons and holes from the slopes of the linear parts in the charge-collection plots. Using

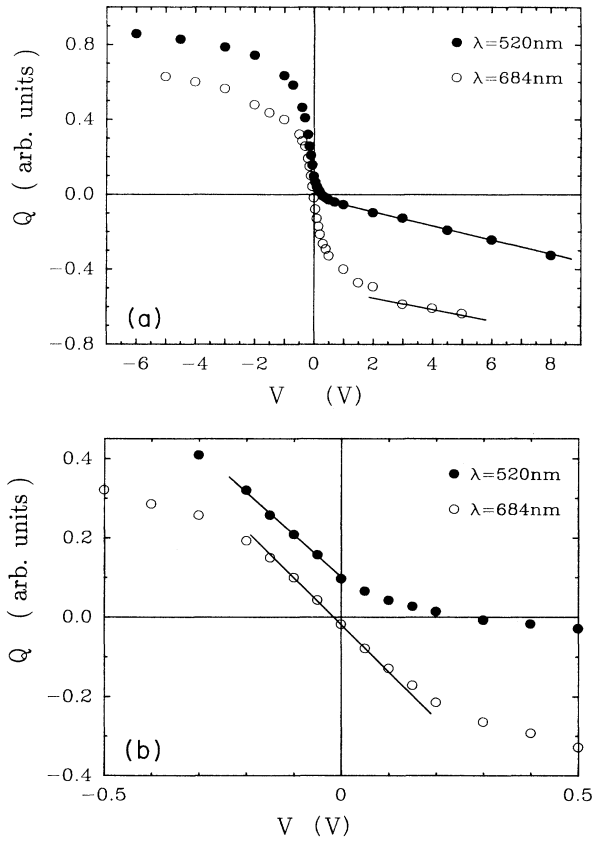

FIG. 6. (a) Photocharge Q collected at 50 μs as a function of the applied voltage V for an annealed a-Si:H specimen (cf. sample 5 in Table I). The photocharge is shown for surface (520 nm) and uniform (684 nm) generation of the photocarriers. (b) Expansion of the region of (a) near $V=0$. Note the substantial collection at $V=0$ from internal fields for the surface-absorbed case. The slopes of the straight lines in (a) and (b) were used to estimate mobility-lifetime products for holes and electrons, respectively.

the estimate of Q_0 obtained from the photocharge at large negative bias, we found using the straight lines drawn in Fig. 6 the values $\mu\tau_e = 1.6\times10^{-7}$ cm^2/V and $\mu\tau_h = 5.0\times10^{-9}$ cm^2/V.

When uniform absorption is used the charge collection for both polarities is symmetrical; this reflects the fact that the initial distributions are equidistant from the two electrodes. Both electrons and holes contribute to the collected charge. We again estimated mobility-lifetime products from these data. To estimate Q_0 we used the following procedure. The linear dependence of Q upon V between 3 and 5 V is due to hole motion, since electrons have already swept out with these voltages. We extrapolated this linear region back to the origin to obtain an estimate of $Q_0/2$. We then estimated the electron mobility-lifetime product at 50 μs from the linear part of the charge-collection plot shown in Fig. 6(b). We obtained $\mu\tau_e = 1.8\times10^{-7}$ cm^2/V. The value is comparable to the result obtained using 520-nm illumination.

The effects of the internal electric fields (collected charge at $V=0$) for the two illuminations can also be seen in Fig. 6(b). The effect is stronger when surface illumination is used. The value of $Q(0)$ can be used with Eq. (6) to obtain the displacement of electrons due to internal fields; we estimate a displacement of about 0.4 μm. This subject is also treated in Refs. 31 and 33. When uniform illumination is used the carriers are distributed uniformly in the specimen. Internal fields are smaller near the middle of the specimen, and in addition the effects of the front and back Schottky barriers tend to cancel. As noted in Sec. V, we only consider mobility-lifetime estimates to be valid when based on data for which the photocarrier drift is much larger than drift attributable to internal fields.

We have performed these measurements for nearly all the specimens described in Table I. In Fig. 7 we show the correlation of the deep-trapping mobility-lifetime products for electrons $\mu\tau_{e,t}$ and holes $\mu\tau_{h,t}$ measured using surface-absorbed illumination (520 nm). The photocharge for the electrons was measured at 10 μs; somewhat longer times were used for holes in better specimens to assure that deep trapping had in fact occurred (cf. Table I). Our results, that in undoped a-Si:H specimens the electron deep-trapping mobility-lifetime products are about ten times bigger than those of holes, are consistent with previous measurements by Street, Zesch, and Thompson.[42]

In Fig. 8 we show the correlation of the electron deep-trapping mobility-lifetime products $\mu\tau_{e,t}$ measured for surface- (520 nm, $\mu\tau^G_{e,t}$) and uniformly absorbed (684 nm, $\mu\tau^R_{e,t}$) light. The photocharge was estimated at 10 μs, and the $\mu\tau$ products were estimated as for Figs. 6(a) and 6(b). The agreement of the two $\mu\tau$ products under uniformly absorbed light and surface-absorbed light is satisfactory. These measurements confirm that either uniform or surface-absorbed illumination can be used to estimate $\mu\tau_{e,t}$ in undoped a-Si:H; the possibility arises primarily because hole transport is relatively unimportant. In principle it would be possible to estimate $\mu\tau_{h,t}$ using homogeneous illumination as well, but we did not investigate

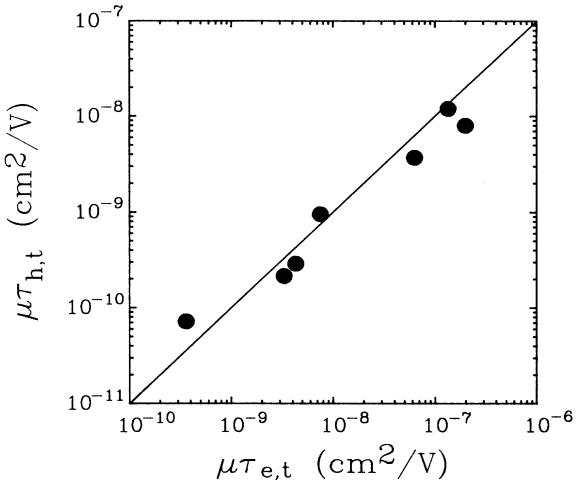

FIG. 7. Correlation of the deep-trapping mobility-lifetime product for electrons $\mu\tau_{e,t}$ and holes $\mu\tau_{h,t}$ using sandwich electrodes for a variety of undoped a-Si:H specimens; also see Table I. Surface-absorbed light (520 nm) was used for the photogeneration of both electrons and holes.

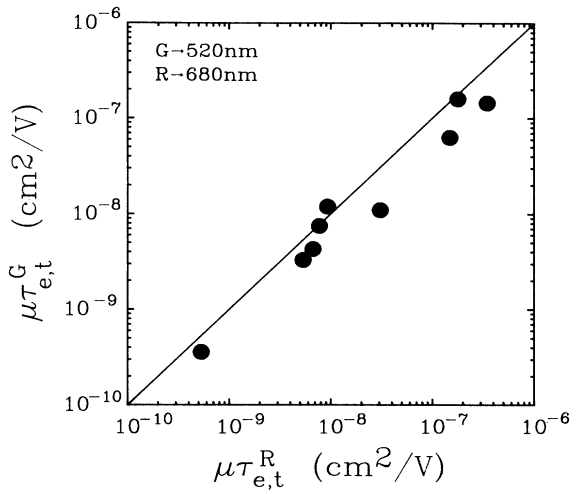

FIG. 8. Correlation of the electron deep-trapping mobility-lifetime product measured with two illumination wavelengths for sandwich electrodes on several a-Si:H specimens. $\mu\tau^{G}_{e,t}$ was measured using 520 nm (surface absorbed). $\mu\tau^{R}_{e,t}$ was measured using 680 nm (uniformly absorbed). See also Table I.

this possibility further.

The $\mu\tau$ products corresponding to surface absorption were systematically smaller than those corresponding to uniform absorption. We speculate that trapping of electrons within the depletion layer reduces the estimate of $\mu\tau_{e,t}$. The effect is obviously largest for surface illumination; additional measurements using 450-nm illumination gave still lower values of $\mu\tau_{e,t}$. These findings are consistent with earlier reports by Spear[20] and Wyrsch *et al.*[43]

[1]N. F. Mott and E. A. Davis, *Electronic Processes in Non-Crystalline Materials,* 2nd ed. (Clarendon, Oxford, 1979).
[2]W. Spear and C. S. Cloude, Philos. Mag. Lett. **55**, 271 (1987).
[3]M. A. Parker and E. A. Schiff, Phys. Rev. B **37**, 10426 (1988).
[4]J. Kočka, E. Šipek, E. Štika, H. Curtins, and G. Juška, J. Non-Cryst. Solids **114**, 336 (1989).
[5]J. Kočka, C. Nebel, and C. D. Abel, Philos. Mag. B **63**, 221 (1991).
[6]J. Bullot, P. Cordier, M. Gauthier, and K. Haddab, J. Non-Cryst. Solids **90**, 195 (1987).
[7]W. Spear, J. Non-Cryst. Solids **1**, 197 (1969).
[8]G. Pfister and H. Scher, Adv. Phys. **27**, 727 (1978).
[9]E. A. Schiff and M. A. Parker, Phys. Rev. Lett. **60**, 1454 (1988).
[10]G. Seynhaeve, R. P. Barclay, and G. J. Andriaenssens, J. Non-Cryst. Solids **97&98**, 607 (1987).
[11]T. Tiedje, in *Hydrogenated Amorphous Silicon II,* edited by J. D. Joannopoulos and G. Lucovsky (Springer-Verlag, New York, 1984), p. 261 and references therein.
[12]J. Marshall, R. A. Street, and M. Thompson, Philos. Mag. **54**, 51 (1986).
[13]W. Spear, in *Amorphous Silicon and Related Materials,* edited by H. Fritzsche (World Scientific, Singapore, 1988), p. 721.
[14]Homer Antoniadis and E. A. Schiff, Phys. Rev. B **43**, 13957 (1991).
[15]J. Orenstein, M. Kaster, and V. Vanivov, Philos. Mag. B **46**, 23 (1982).
[16]M. Silver, G. Schöenherr, and H. Bässler, Phys. Rev. Lett. **48**, 352 (1982).
[17]H. Scher, in *Photoconductivity and Related Phenomena,* edited by J. Mort and D. M. Pai (Elsevier, Amsterdam, 1976), p. 71.
[18]S. P. Hotaling, Homer Antoniadis, and E. A. Schiff, Sol. Cells **27**, 357 (1989).
[19]R. A. Street, Appl. Phys. Lett. **41**, 1060 (1982).
[20]W. Spear, J. Non-Cryst. Solids **59&60**, 1 (1983); **66**, 163 (1984).
[21]P. Kirby and W. Paul, Phys. Rev. B **29**, 826 (1984).
[22]R. Könenkamp, J. Non-Cryst. Solids **77&78**, 643 (1985).
[23]E. A. Schiff, M. A. Parker, and K. A. Conrad, *Amorphous Silicon Technology,* edited by Arun Maday, M. J. Thompson, P. C. Taylor, P. G. LeComber, and Y. Hamakawa, MRS Symposia Proceedings No. 118 (Materials Research Society, Pittsburgh, 1988), p. 477.
[24]S. P. Hotaling, Homer Antoniadis, and E. A. Schiff, J. Non-Cryst. Solids **114**, 420 (1989).
[25]Homer Antoniadis and E. A. Schiff, *Amorphous Silicon Technology,* edited by P. C. Taylor, M. J. Thompson, P. G. LeComber, Y. Hamakawa, and Arun Maday, MRS Symposia Proceedings No. 192 (Materials Research Society, Pittsburgh, 1990), p. 293.
[26]E. A. Schiff, Philos. Mag. Lett. **55**, 87 (1987).
[27]K. A. Conrad and E. A. Schiff, Solid State Commun. **60**, 291

(1986).
[28]R. Könenkamp, S. Muramatsu, H. Itoh, S. Matsubara, and T. Shimada, Jpn. J. Appl. Phys. **29**, L2155 (1990).
[29]K. Conrad, Ph.D. thesis, Syracuse University, 1988.
[30]M. A. Parker, Ph.D. thesis, Syracuse University, 1988.
[31]R. A. Street, Phys. Rev. B **27**, 4924 (1983).
[32]V. K. Hecht, Z. Phys. **77**, 235 (1932).
[33]R. Vanderhagen and C. Longeaud, *Amorphous Silicon Technology,* edited by Arun Maday, M. J. Thompson, P. C. Taylor, Y. Hamakawa, and P. G. LeComber, MRS Symposia Proceedings No. 149 (Materials Research Society, Pittsburgh, 1989), p. 357.
[34]S. Hasegawa and Y. Imai, Philos. Mag. B **46**, 239 (1982).
[35]B. Aker, Philos. Mag. B **55**, 313 (1987).
[36]M. Tanielian, Philos. Mag. B **45**, 435 (1982).
[37]W. B. Jackson, R. A. Street, and M. J. Thompson, Solid State Commun. **47**, 435 (1983).
[38]M. A. Parker and E. A. Schiff, J. Non-Cryst. Solids **97&98**, 627 (1987).
[39]K. D. Mackenzie and W. Paul, J. Non-Cryst. Solids **97&98**, 1055 (1987).
[40]M. Vaněček, J. Kočka, E. Šipek, and A. Třiska, J. Non-Cryst. Solids **114**, 447 (1989).
[41]H. T. Grahn, Ph.D. thesis, Brown University, 1988.
[42]R. A. Street, J. Zesch, and M. J. Thompson, Appl. Phys. Lett. **43**, 672 (1983).
[43]N. Wyrsch, P. Roca Cabarrocas, S. Wagner, and V. Viret, in Ref. 25, p. 329.

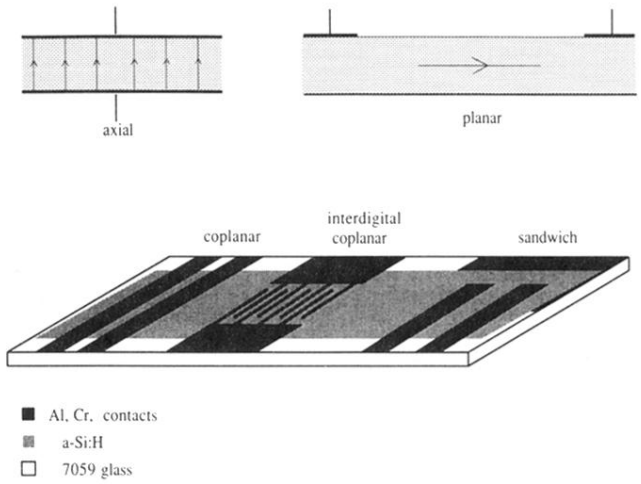

FIG. 1. Schematic illustration of the three types of electrode structures used for this research; drawings are not to scale. The upper portion of the figure illustrates the direction of axial and planar electric fields relative to the growth axis of the thin film.